Numerical Study of Flux Models for CO_2: Enhanced Natural Gas Recovery and Potential CO_2 Storage in Shale Gas Reservoirs

Nilay J. Prajapati[1] and Patrick L. Mills[*1]
[1]Department of Chemical and Natural Gas Engineering, Texas A&M University-Kingsville,
*Corresponding author: Texas A&M University-Kingsville, MSC 188, 700 University Blvd, Kingsville TX 78363-8202, USA. Email: Patrick.Mills@tamuk.edu

Abstract: Gas production from shale reservoirs has become a major source of fossil energy in the United States (US EIA, 2011). Because of their low porosity and ultra-low permeability, shale reservoirs often reach peak production in a very early stage compared to conventional sandstone reservoirs (Naik, 2003). Various attempts have been made to model the fluid flow behavior in shale reservoirs (Fathi & Akkutlu, 2011; Guo *et al.*, 2014; Javadpour, 2009; Sun *et al.*, 2014). Slip flow, diffusion, and adsorption-desorption are typically considered as the primary flow mechanisms in shale nano-pores while flow in fractures can be described by Darcy's law. The emphasis of this paper is to model flow for a shale reservoir system at the micro to nanoscale scale using COMSOL Multiphysics. Propagation of binary CH_4-CO_2 mixture in the shale matrix is analyzed using four different flux models, namely, the Wilke, Wilke-Bosanquet, Maxwell-Stefan and Dusty Gas models (Solsvik & Jakobsen, 2013). The performance of these flux models is compared by accounting for both inter-molecular and gas-rock interactions. The results show that flux models must account for Knudsen diffusion due to the presence of shale nano-pores. When Knudsen diffusion is not present in the flux model, such as in the Wilke and Maxwell-Stefan models, the gas transport is approximately 10 times greater than the Wilke-Bosanquet and Dusty Gas flux models where Knudsen diffusion is included. Shale also has a greater affinity for CO_2 which can result into enhanced production of CH_4.

Keywords: Shale gas, flux models, COMSOL, simulation

1. Introduction

The US EPA has reported about 5% increase in carbon dioxide (CO_2) emissions in the US between 1990 and 2012 (EPA 430-R-12-001, 2012). This increase is believed to be responsible for current global warming trends. Reduction of CO_2 in the atmosphere is an important environmental challenge. One of the most effective ways to reduce CO_2 is to utilise geological CO_2 storage. Technologies being developed for geologic storage are focused on five storage types: oil and gas reservoirs, saline formations, un-mineable coal seams, basalts, and organic-rich shales (NETL, 2013). Geological storage involves direct injection of CO_2 into underground geological formations.

Shales are relatively low in porosity (0.08-0.12) and have ultra-low permeability (10^{-10} to 10^{-12} Darcy). They consist of pores with a wide range of sizes, which often leads to multimodal pore-size distribution (Akkutlu & Fathi, 2012). Existence of nano-pores in shales was identified by Fathi and Akkutlu (2011), Javadpour (2009) and Kang *et al.* (2011). Diversity of minerals that make up shale, such as clays, carbonates, and organic material (*i.e.*, kerogen), add to its heterogeneous nature (Akkutlu & Fathi, 2012).

US shale gas production has grown rapidly in recent years (US EIA, 2011), which has been led by new developments in hydraulic fracturing and horizontal drilling. However, it has been found that shale gas reservoirs reach peak production in relatively short time span as compared to conventional sandstone reservoir (Naik, 2003). Technological advancements, such as re-frac, have been implemented as a possible approach for sustaining the well production rate for a longer time period (Jacobs, 2014).

The high adsorption capacity of shale for CO_2 compared to CH_4 was identified by Kang *et al.* (2011). When CO_2 is injected into gas-bearing shale reservoirs, it enhances the recovery of methane (CH_4), which suggests that shale reservoirs may be useful for storage. In addition, simultaneous recovery of CH_4 while CO_2 is being stored is attractive because it can lead to the reduction of atmospheric CO_2 while also offsetting costs of capture, compression, transportation, and storage. Kang *et al.* (2011) also showed that CO_2 storage in organic rich shales has added advantages because the organic matter acts as a molecular sieve, thereby

allowing CO_2, with its molecular geometry, to reside in small pores that cannot be accessed by other naturally occurring gases. In addition, the molecular interaction energy between the organics and CO_2 molecules is higher, which leads to enhanced adsorption of CO_2 (Kang *et al.*, 2011). Moreover as gas wells are depleted, these shales could become a possible candidate for sequestration CO_2.

Advanced Resources International developed a simulation platform called COMET3 to assess Eastern gas shales for CO_2 storage (Godec, 2013). ECLIPSE and CMG GEM simulation engines are also used for reservoir modelling of CO_2 injection in Devonian gas shale. C. Guo *et al.* (2014) emphasised modelling shale gas flow mechanisms using the Dusty Gas flux model using COMSOL. H. Sun *et al.* (2014) extended the application of the Dusty Gas model for modelling CO_2-shale gas physics.

In this work, four different flux models for describing gas transport are considered. The equations are developed on the basis of a dual porosity model and coupled with extended Langmuir adsorption (Sun *et al.*, 2014). The model equations are solved using the COMSOL PDE module using the binary CH_4-CO_2 mixture in the shale matrix.

2. Defining shale gas model

Javadpour (2009) reported that gas flow in shale gas reservoirs cannot be described simply by Darcy's law because of small pores whose mean diameters are on the order of nanometers. Slip flow, diffusion and adsorption-desorption are considered as the primary flow mechanisms in shale nano-pores. Two classes of approaches are commonly used for describing fluid flow in fractured systems: dual porosity/permeability and discrete fracture model (Guo *et al.*, 2014). Here, the dual-porosity model is considered, which is comprised of a "matrix" system that is defined by low porosity and ultra-low permeability and a "fracture" system, which is defined by relatively low porosity but high permeability. The matrix system is composed of inorganic matrix embedded with heterogeneous distribution of organic-rich material called "kerogen". The kerogen stores the majority of gas as an adsorbed phase.

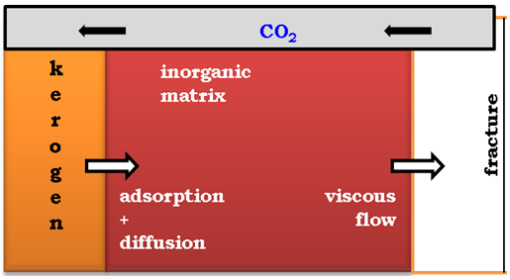

Figure 1. Schematic of shale matrix-fracture model and fluid path during injection

Fathi and Akkutlu (2012), Leahy-dios *et al.* (2011) and Mengal and Wattenbarger (2011) showed the importance of adsorption in shale nano-pores for gas storage and transport. The molecules in the vicinity of pore wall follow the hopping mechanism and further transit to surface and molecular diffusion. The mass balance equation should consider both adsorption-desorption as well as diffusion as the primary flow mechanisms for fluid flow in the matrix and kerogen. The current work considers flow of a binary mixture consisting of CH_4 and CO_2 in the kerogen-inorganic composite matrix.

Model Assumptions:

The key model assumptions are: (1) all gas species follow the ideal gas law; (2) the reservoir temperature remains constant; (3) a single-phase gas flow exists; (4) no variation occurs in the rock compressibility; (5) the horizontal and vertical permeabilities are assumed to be equal (isotropic media); and (6) the porosity of both media (matrix and fracture) remain constant.

To describe the flow through these systems, four specie-flux models are considered: Wilke model, Wilke-Bosanquet model, Maxwell-Stefan model and the Dusty-gas model (Solsvik & Jakobsen, 2013). The final expressions for the fluxes of each model are:

Wilke model:

$$\boldsymbol{N_i} = \left(-\boldsymbol{D_{ei,m}}\boldsymbol{\nabla C_i}\right);\ \boldsymbol{D_{ei,m}} = \frac{\mathbf{1}}{\left(\sum_{\substack{j=1 \\ j\neq i}}^{n}\left(x_j/D_{ij}^{e}\right)\right)} \quad \text{.....(1)}$$

Wilke Bosanquet model:

$$\boldsymbol{N_i} = \left(-\boldsymbol{D_{i,eff}}\boldsymbol{\nabla C_i}\right);\ \frac{\mathbf{1}}{\boldsymbol{D_{i,eff}}} = \frac{\mathbf{1}}{\boldsymbol{D_{ei,m}}} + \frac{\mathbf{1}}{\boldsymbol{D_{ei,k}}} \quad \text{.....(2)}$$

Maxwell-Stefan model:

$$N_i = \frac{-\nabla C_i + \sum_{\substack{j=1 \\ j\neq i}}^{n} \frac{x_i N_j}{D_{ij}^e}}{\sum_{\substack{j=1 \\ j\neq i}}^{n} \frac{x_j}{D_{ij}^e}} \quad \text{.....(3)}$$

Dusty-Gas model:

$$N_i = \frac{\sum_{\substack{j=1 \\ j\neq i}}^{n} \frac{x_i N_j}{D_{ij}^e} - \frac{C_i v^*}{D_{ei,k}} - \nabla C_i}{\sum_{\substack{j=1 \\ j\neq i}}^{n} \frac{x_j}{D_{ij}^e} + \frac{1}{D_{ei,k}}}; \quad v^* = -\frac{\varepsilon\, d_{pore}^2}{32\,\tau\,\mu} \nabla P \quad \text{....(4)}$$

In the above equations, N_i is the molar flux of component *i*, x_i is mole fraction of component *i*, C_i is concentration (mol/m^3) of component *i*, and $\mathbf{D_{ij}^e}$ is the binary molecular diffusion coefficient of specie i in specie j, which is calculated using the Chapman-Enskog correlation (Ho and Webb, 2006). The effective Knudsen diffusion coefficient of specie i ($\mathbf{D_{ei,k}}$) is calculated using correlation given in Sun *et al.* (2014). The parameter $\boldsymbol{\varepsilon}$ in Eq.(4) is the porosity, d_{pore} is pore diameter and $\boldsymbol{\tau}$ is tortuosity.

Governing equations for flow in the matrix:

The mass balance for specie i in the kerogen-inorganic composite matrix system is:

$$\frac{\partial\left(\rho\varphi_m + \rho_q(1-\varphi_m)\right)_i}{\partial t} + \nabla \cdot (\rho u)_{m,i} = 0 \quad \text{.....(5)}$$

where i = 1 (Methane, CH_4) and i = 2 (Carbon Dioxide, CO_2), ρ is gas density at reservoir temperature and pressure, φ_m is matrix porosity, $(\rho u)_{m,i}$ is mass flux of component i in matrix, ρ_q is gas density of adsorbed gas, which is defined as follows (Sun *et al.*, 2014):

$$\rho_{q,i} = \frac{\rho_S M_i}{V_{std}} * q_{ads,i} \quad \text{.....(6)}$$

In Eq.(6), ρ_s is the shale rock density, M_i is the molar mass of component i, V_{std} is the standard molar volume and $q_{ads,i}$ is the amount of gas adsorbed on the rock mass. The latter parameter is obtained from the extended Langmuir adsorption isotherm.

$$q_{ads,i} = \frac{V_{L,i} B_i P_i}{1 + \sum_{j=1}^{n} B_j P_j} \quad \text{.....(7)}$$

The above equations can be expressed in terms of the partial pressure for each component using

$$\rho_i = \frac{P_i M_i}{Z_i R T}, \quad \text{where the partial pressure of specie } i \text{ is } P_i = x_i P \quad \text{.....(8)}$$

Here, P denotes the total reservoir pressure at a particular time, Z_i is gas compressibility factor and T is reservoir temperature.

3. Use of COMSOL Multiphysics

The above system of nonlinear equations for fluid flow in the shale nano-pores are solved with COMSOL Multiphysics PDE module using the PARDISO solver. The tolerance factor is set to 0.1 and the maximum number of iterative steps value was set at 5. Both a physics-controlled mesh and a user-controlled mesh calibrated for fluid dynamics wereused. Grid refinement in the injection zone was necessary for accurate numerical simulation. **Table1** in the appendix shows reservoir parameters used in model. Initial conditions for shale model are:

$$P_{m,i}(x,y,t)|_{t=0} = P_i \quad \text{.....(9)}$$

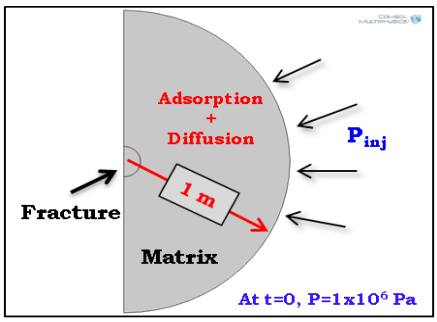

Figure 2. COMSOL Model geometry

The boundary for the solution is $\Gamma = \Gamma_1 + \Gamma_2$, where Γ_1 represents outer boundary for matrix and Γ_2 represents outer boundary for fracture. Therefore, the boundary conditions are:

$$(\rho u)_{m,i}|_{\Gamma_1} = 0 \text{ and } \nabla(\rho u)_{m,i}|_{\Gamma_2} = 0 \quad \text{.....(10)}$$

4. Results and discussion

The initial pressure of the gas reservoir was taken as 1 MPa and the molar volume under standard conditions is 0.0224 m^3/mol. The

Langmuir parameters are taken from Sun *et al.* (2014). The model formulae are transformed into the standard coefficient PDE form in COMSOL and simulated for different flux models. At the injection point, CH_4 and CO_2 are introduced in a molar ratio of 1:1.

Figures 3 to 6 are concentration history plots for all four flux models at matrix-fracture interface. In all cases, the CO_2 profiles show a lag in reaching the injection concentration from initial reservoir concentration compared to the CH_4 profiles. This can be attributed to the higher adsorption strength of shale rock for CO_2. Furthermore, it is also found that Knudsen diffusion has a significant impact on the gas flow in the shale nano-pore system. Introduction of Knudsen diffusion (Wilke-Bosanquet model and Dusty Gas model) causes reduction in transport of the gases within the medium and an increase in the contact time with the rock pore-walls. This enhances the gas-rock interaction, making surface diffusion as the primary flow mechanism for the gas species in the vicinity of the pore-wall. This effect is clearly shown by the Wilke-Bosanquet model.

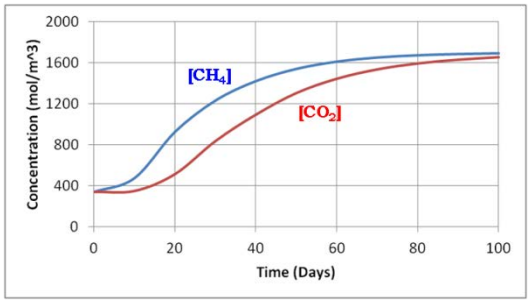

Figure 3. Concentration history plot for Wilke flux model

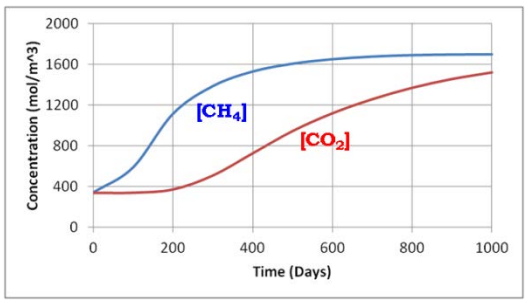

Figure 4. Concentration history plot for Wilke-Bosanquet flux model

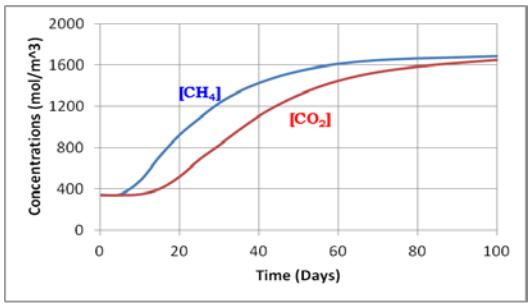

Figure 5. Concentration history plot for Maxwell-Stefan flux model

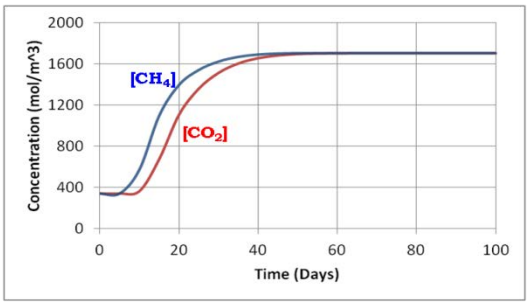

Figure 6. Concentration history plot for Dusty Gas flux model

The 2D results (Figures 7 and 8) show that the highest rate of specie transport is obtained with the Dusty Gas model while the lowest rate is obtained with the Wilke-Bosanquet model. The Dusty Gas model includes convective transport in the porous matrix along with Knudsen diffusion (D_k) and binary molecular diffusion (D_m). Conversely, the Wilke-Bosanquet model incorporates only D_k and D_m. Apart from this, the Dusty Gas model additionally incorporates a relative flux of both the species at a time. As a result, a higher rate of species transport is obtained for both the gas species with the Dusty Gas model when compared to the other flux models whereas a longer characteristic time is obtained for diffusion-driven transport of gas species with the Wilke Bosanquet model.

Both the Maxwell-Stefan and Wilke flux models produce similar concentration profiles that can be mainly attributed to transport by molecular diffusion. However, the flux profiles obtained for both the models are significantly different. This is because Maxwell-Stefan model considers the relative flux of both the species at a time while Wilke model considers only one specie at a time.

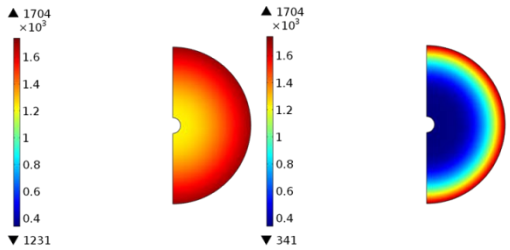

Figure 7. Concentration profile for methane with Wilke flux model (left) and Wilke-Bosanquet flux model (right) through 30 days

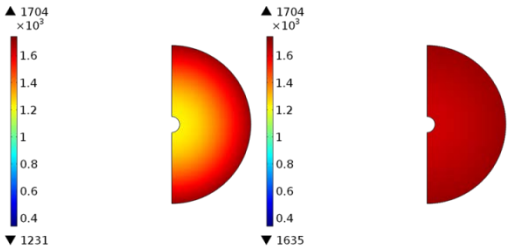

Figure 8. Concentration profile for methane with Maxwell-Stefan flux model (left) and Dusty gas flux model (right) through 30 days

Figures 9 compares the flux profiles for the Wilke, Wilke-Bosanquet, Maxwell-Stefan, and Dusty Gas (without the convective term) models at the matrix-fracture interface. The Dusty Gas model equation is dissected into two parts to analyze the effect of each flow term on the specie transport and compare with other flux models. These parts are: (1) with the convective transport term, and (2) without the convective transport term.

It is noticed that the absence of Knudsen diffusion (D_k) leads to a higher flux. Therefore, a higher flux is observed with the Wilke and Maxwell-Stefan models in Figure 9. When D_k is included in the flow equations (Wilke Bosanquet and Dusty Gas models) both the gas species are retained for a longer time in the matrix, which results in the lower flux. Moreover, shale rock has higher adsorption strength for CO_2. As a result, CO_2 is retained in the adsorbed phase for even a longer period of time. This causes CO_2 to penetrate deeper into the nano-pores and replace the adsorbed CH_4 molecules; improving CH_4 recovery. CO_2 will remain adsorbed to the shale rock surface until a threshold pressure is reached.

Comparison of the Wilke-Bosanquet and Dusty Gas (without convection) models (Figure 10) shows that inclusion of the relative flux term generates a higher flux in the Dusty Gas model. Figure 11 shows a flux plot for a complete Dusty Gas model. The convective transport term significantly increases the flux. This can be attributed to the combined effects of tortuosity, pore size distribution and gas viscosity. It is also deduced that CO_2 has a higher mobility in the shale nano-pore system than CH_4.

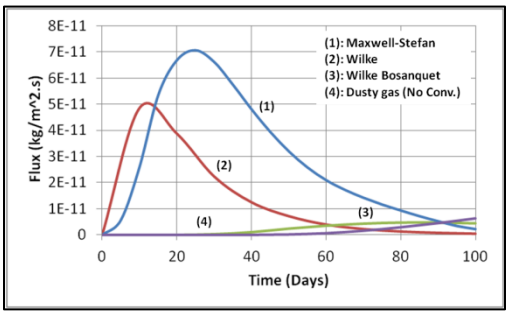

Figure 9. CH_4 flux plot for Wilke, Wilke-Bosanquet, Maxwell-Stefan and Dusty Gas (without convection term) flux models

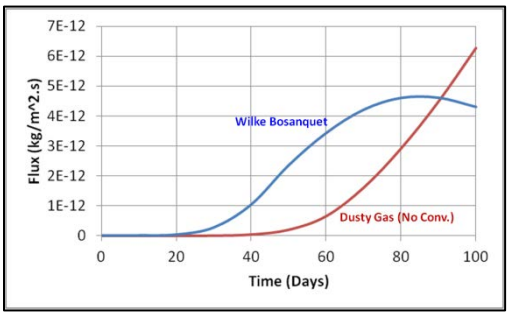

Figure 10. CH_4 flux plot for Wilke Bosanquet and Dusty Gas (without convective term) flux models

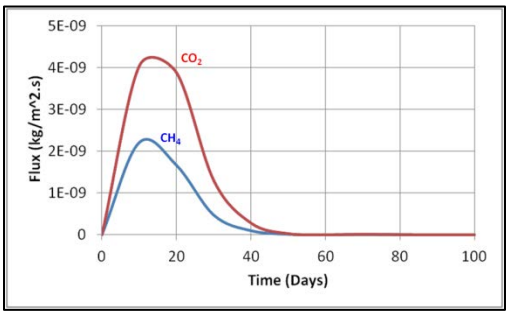

Figure 11. Flux plot for Dusty Gas (with convective term) flux model

5. Conclusions and Future work

The simulation of shale nano-pore system provides quantitative insight into the flow behavior of gaseous species. The dual porosity mathematical model is adopted for the shale reservoir system incorporating multiple mechanisms of adsorption, Knudsen diffusion and binary diffusion. Comparison of four flux models shows how each mechanism can impact the concentration and flux at the matrix-fracture interface. To accurately model the shale nano-pore system, both Knudsen diffusion and binary molecular diffusion along with the pore size distribution should be considered. The Dusty Gas model contains the key transport terms that can properly capture the system physics..

This work can be extended by including other physical phenomena, such as fracture flow mechanics, shale heterogeneity, other gas species and multi-phase flow due to variable pressure, temperature and water concentration.

6. References

Akkutlu, I.Y. and Fathi, E., Multiscale Gas Trasport in Shales with Local Kerogen Heterogeneities. *SPE Journal*, 1002–1011 (2012)

Fathi, E. and Akkutlu, I.Y. Mass Heterogeneity Effects on Gas Transport and Adsorption in Coalbed and Shale Gas Reservoirs. *Transp Porous Med*, **80,** 281–304 (2011)

Fathi, E., Tinni, A. and Akkutlu, I.Y. Correction to Klinkenberg Slip Theory for Gas Flow in Nano-capillaries. *Intl. Journal of Coal Geology* **103**, 51–59 (2012)

Godec, M., Koperna, G., Petrusak, R. *et al.* Assessment of Factors Influencing CO2 Storage Capacity and Injectivity in Eastern U.S. Gas Shales, *Energy Procedia* **37**, 6644–6655 (2013)

Guo, C., Wei, M., Chen, H. *et al.* Improved Numerical Simulation for Shale Gas Reservoirs. Paper OTC 24913 presented at Offshore Technology Conference, Kuala Lumpur, Malaysia. (2014)

Ho, C. and Webb, S. *Gas Transport in Porous Media*, Springer, The Netherlands (2006)

Jacobs, T. Renewing Mature Shale Wells Through Refracturing, *SPE* (2014)

Javadpour, F. Nanopores and Apparent Permeability of Gas Flow in Mudrocks. *Journal of Cdn Pet. Tech*., **48**, 16–21 (2009)

Jiang, J., Shao, Y. and Younis, R. Development of a Multi-Continuum Model for Enhanced Gas Recovery and CO_2 Storage in Fractured Shale Gas Reservoirs, Paper SPE 169114, presented at SPE Improved Oil Recovery Symposium, Tulsa, Oklahoma, USA (2014)

Kang, S.M., Fathi, E., Ambrose, R.J., *et al.* Carbon Dioxide Storage Capacity of Organic-Rich Shales. Paper SPE 134583, presented at SPE Annual Technical Conference and Exhibition, Florence, Italy. (2011)

Leahy-Dios, A., Das, M. and Agarwal, A. *et al.* Modeling of Transport Phenomena and Multicomponent Sorption for Shale Gas and Coalbed Methane in an Unstructured Grid Simulator. Paper SPE 147352 presented at SPE Annual Technical Conference and Exhibition, Denver, Colorado, USA (2011)

Mengal, S.A., and Wattenbarger, R.A. Accounting for Adsorbed Gas in Shale Gas Reservoirs. Paper SPE 141085, presented at SPE Middle East Oil and Gas Show and Conference, Manama, Bahrain (2011)understanding

Naik, G. C. Tight Gas Reservoirs – An Unconventional Natural Energy Source for the Future. SPE-Italy (2003)

NETL, Optimizing and Quantifying CO_2 Storage Resource in Saline Formations and Hydrocarbon Reservoirs. Project DE-FE0009114 (2013)

Solsvik, J., Jakobsen, H., Multicomponent Mass Diffusion in Porous Pellets: Effects of Flux Models on the Pellets Level and Impacts on the Reactor Level. Application to Methanol Synthesis, Can. *Journal of Chem. Eng.*, **91**, 66–76 (2013)

Sun, H., Yao, J., Gao, S. *et al.* Numerical Study of CO_2 Enhanced Natural Gas Recovery and Sequestration in Shale Gas Reservoirs, *Intl. Journal of Greenhouse Gas Control*, **19**, 406–419 (2014)

U.S. Energy Information Administration. Review of Emerging Resources: U.S. Shale Gas and Shale Oil Plays, *Independent Statistics & Analysis* (2011)

U.S. Environmental Protection Agency. Inventory of U.S. Greenhouse Gas Emissions and Sinks: 1990-2010. EPA 430-R-12-001, Washington, DC (2012)

7. Appendix

Table 1: Reservoir parameters

Molar mass of methane, kg/mol	0.016
Molar mass of carbon dioxide, kg/mol	0.044
Permeability, m^2	1.0×10^{-19}
Porosity	8.0 %
Rock density, kg/m^3	2560
Absolute temperature, K	353
Gas deviation factor (Z_s) of mixture	1.0
Rock compressibility, Pa^{-1}	1×10^{-5}
Langmuir pressure of CH_4, Pa	3.05×10^6
Langmuir pressure of CO_2, Pa	1.68×10^6
Langmuir volume of CH_4, $std.m^3/kg$	9.80×10^{-4}
Langmuir volume of CO_2, $std.m^3/kg$	1.91×10^{-3}